Sub-100 nm 3-D fluorescence lifetime imaging using time correlated single photon counting detection and multifocal multiphoton excitation

S. Kumar, C. Dunsby, P. A. A. De Beule, D. M. Owen, U. Anand, P. M. P. Lanigan, R. K. P. Benninger, D. M. Davis, M. A. A. Neil, P. Anand, C. Benham, A. Naylor, and P. M. W. French

Cite as: Optics Express 15, 12548 (2007) https://doi.org/10.1364/OE.15.012548

The interaction of matter and light is one of the fundamental processes occurring in nature, and its most elementary form is realized when a single atom interacts with a single photon. Reaching this regime has been a major focus of research in atomic physics and quantum optics for several decades and enables fascinating applications such as 3-D fluorescence imaging. Here we report a multifocal multiphoton time-correlated single photon counting (TCSPC) fluorescence lifetime imaging (FLIM) microscope system that uses a 16 channel multi-anode PMT detector. Multiphoton excitation minimizes out-of-focus photobleaching, multifocal excitation reduces non-linear in-plane photobleaching effects and TCSPC electronics provide photon-efficient detection of the fluorescence decay profile. TCSPC detection is less prone to bleaching- and movement-induced artefacts compared to wide-field time-gated or frequency-domain FLIM. This microscope is therefore capable of acquiring 3-D FLIM images at significantly increased speeds compared to single beam multiphoton microscopy and we demonstrate this with live cells expressing a GFP tagged protein. We also apply this system to time-lapse FLIM of NAD(P)H autofluorescence in single live cells and report measurements on the change in the fluorescence decay profile following the application of a known metabolic inhibitor.

1. Introduction

Multiphoton microscopy [**1**, **2**] enables high resolution 3-D images of fluorescent samples to be obtained for applications in biomedical research. The oft-cited advantages of multiphoton microscopy over single-photon confocal microscopy include an increased penetration depth due to the decreased scattering of the excitation light at longer wavelengths and low out-of-focus photobleaching and photodamage. Multiphoton excitation also provides a convenient method for imaging fluorophores that are excited in the UV, e.g. for imaging cellular NAD(P)H autofluorescence [**3**].

Fluorescence lifetime imaging (FLIM) is an increasingly widely applied spectroscopic technique [**4–6**] that is often implemented on multiphoton microscope systems. Imaging fluorescence lifetime can provide information on the localisation of specific fluorophores and variations in fluorophore environment such as ion concentration, pH, oxygen concentration, refractive index, viscosity, temperature etc [**4**]. One advantage of FLIM is that it is insensitive to fluorophore concentration, as it

does not require absolute measurements of the fluorescence intensity. FLIM can also be employed for detection of Förster (fluorescence) resonance energy transfer (FRET) between pairs of fluorophores, especially for studying the interactions and dynamics of proteins within cells [**7**, **8**]. However, conventional FLIM microscopy, particularly with single beam multiphoton excitation, often requires relatively long acquisition times, which can limit the use of this technique, especially when imaging live-cells that may be compromised if higher excitation intensities are used.

In this paper we report, to the best of our knowledge, the first multifocal multiphoton time-correlated single photon counting (TCSPC) FLIM microscope. This system produces minimal photobleaching during the acquisition of 3-D FLIM images and can also be applied to optically-sectioned time-lapse FLIM of live cells. Fluorescence excited at each of 16 foci is recorded on a separate element of a 16 channel photomultiplier tube (PMT) and the photon arrival times are recorded using TCSPC electronics. The multifocal multiphoton TCSPC FLIM system can be considered in two limits: highly fluorescent and weakly fluorescent samples. In the case of highly fluorescent samples, the system could be implemented with separate detection electronics for each of the 16 detector channels in order to achieve the maximum possible photon count rate. In the case of weakly fluorescent samples, the multifocal TCSPC FLIM system can provide a 16-fold increase in the signal compared to a single beam multiphoton system using only a single set of detection electronics. We demonstrate FLIM of live cells expressing GFP to illustrate the potential of this system for studying the 3-D distribution of proteins and protein-protein interactions via FRET, e.g. [**9**]. We also show the application of this instrument to time-lapse FLIM of cellular NAD(P)H autofluorescence, imaging single cells during stimulation with the metabolic inhibitor NaCN. Image acquisition time is an important factor for many biological experiments and limits both the (macroscopic) temporal resolution that can be achieved and the number of samples that can be studied in a given time period. The microscope system presented here provides a method to increase the imaging rate for 3-D multiphoton FLIM experiments.

1.1 Photobleaching and phototoxicity

Photobleaching is an important consideration for all types of fluorescence microscopy and places a fundamental limit on the amount of information that can be obtained from any sample. Multiphoton microscopy is known to produce enhanced (nonlinear) photobleaching in the focal plane [**10**, **11**], i.e. a photobleaching rate that scales nonlinearly with amount of fluorescence signal generated. For example, recent results for endogenous cellular NAD(P)H fluorescence show a fourth-power dependence of photobleaching rate with respect to excitation power [**12**]. Although the exact nature of the photobleaching mechanism during multiphoton excitation will depend on the fluorophore in question, in many cases it involves the absorption of a photon by a molecule that is in an excited state [**10**, **13**]. Non-linear photobleaching restricts the rate at which fluorescence can be excited in a multiphoton microscope and also limits the total signal that can be detected. In-plane photobleaching

in multiphoton microscopy can be greater than that due to single-photon excitation for the same amount of generated fluorescence signal [**10**]. However, single photon confocal microscopy bleaches the sample uniformly throughout the axial extent of the sample (assuming linear photobleaching processes) [**14**, **15**], while multiphoton microscopy only bleaches in the focal plane. Therefore, multiphoton microscopy produces less overall photobleaching of the sample compared to single photon confocal microscopy when a 3-D image with a large number of z-steps is required.

Two phenomena that are closely related to photobleaching are photodamage and phototoxicity; these limit the amount of excitation power that can be used in both single and multiphoton microscopy if sample viability is to be maintained. For single-photon excitation, photobleaching and photodamage effects occur throughout the illumination volume. With multiphoton microscopy, linear absorption of excitation light by water does not cause a significant increase in sample temperature at typical average powers used and therefore does not contribute significantly to photodamage [**16**, **17**]. However, a range of multiphoton photodamage and phototoxicity mechanisms exist that depend on the excitation wavelength and fluorophores involved [**18–20**]. Generally, photodamage relates to direct physical damage to the sample, e.g. generation of DNA strand breaks or plasma formation, whereas phototoxicity relates to the generation of chemical species, e.g. reactive oxygen species, that go on to cause damage to the cell. Phototoxicity in multiphoton microscopy has been shown to increase with excitation power according to a power law dependence of 2 for unlabelled cells [**18**] and for cells labelled with calcium sensitive dyes at low excitation power levels [**21**]. Highly nonlinear phototoxicity and photodamage effects with a power law dependence of >2 have also been reported [**20**, **21**], particularly when higher excitation powers are employed.

1.2 Multifocal multiphoton microscopy

The ultrafast excitation sources most commonly used in multiphoton microscopy are based on mode-locked Ti:Sapphire lasers that typically provide average output powers of > 1 W, which is far more than should be applied at the sample plane in conventional single-beam multiphoton microscopy. One way to make use of the excess power yet retain diffraction limited axial resolution is to utilize multiple excitation foci [**22–24**]. If a multifocal multiphoton microscope utilizes *n* beams each with the same average power as employed in a single beam system, then the total fluorescence signal generated per unit time increases by a factor of *n*. The ratio of the number of fluorescence photons generated per photobleaching event remains the same, regardless of the number of excitation beams and is therefore independent of the amount of fluorescence signal excited. A further less commonly considered factor for multiphoton microscopy is the reduction in resolution caused if the fluorescence signal from the focal volume becomes saturated [**25**]. By dividing the incident power between multiple foci, this effective loss of resolution is reduced. The use of multiple excitation foci to achieve higher fluorescence signals with lower excitation intensities may also have the potential to minimize phototoxic effects when imaging live cells.

1.3 Fluorescence lifetime imaging

FLIM methodologies may be divided into three categories: direct 'electronic' detection of the decay profile, time-gating and frequency domain techniques [**5**]. Methods for direct electronic detection of the fluorescence decay include TCSPC [**26–28**] and streak camera based techniques [**29**, **30**]. These methods provide high photon detection efficiencies as, in principle, all collected photon events are recorded and an appropriate decay model can be directly fitted to the experimental data. Direct electronic detection also reduces the possibility of artefacts in the fluorescence decay caused by bleaching or sample movement during the acquisition, which can occur during time or frequency domain measurements that require sequential image acquisitions at varying delay times or phase-shifts. This is particularly important when following changes in fluorescence lifetime that are accompanied by changes in fluorescence intensity. Beam splitting optics for single-shot capture of multiple images can be used to overcome this limitation of wide-field FLIM, e.g. [**31**], however, the necessary optics and image registration are relatively complex.

In conventional single beam multiphoton microscopes FLIM is most commonly realised using TCSPC, which is relatively low-cost and straightforward to implement. This approach provides high quality FLIM data, but the sequential pixel acquisition and limitations on excitation power imposed by photobleaching or photodamage considerations can make it relatively slow for some applications, e.g. live cell imaging. Ultimately, the rate at which photons can be detected using TCSPC is limited by photon pile-up and the dead-time of the detection electronics [**32**] and, if necessary, these effects can be mitigated through the use of multiple TCSPC detectors and detection electronics modules, or through the use of a multiple time-gate photon-binning method [**33**].

1.4 FLIM in multifocal multiphoton microscopes

FLIM has been implemented in multifocal multiphoton microscope systems using wide-field time-gated multi-channel plate intensifiers [**34–36**] and in a hyperspectral imaging streak camera configuration [**37**]. The sampling nature of time-gated detection results in a decrease in the fluorescence detection efficiency, particularly if complex fluorescence decay profiles are to be resolved via the acquisition of many time-gated images. Imaging streak cameras do not gate the fluorescence signal and can achieve higher photon economy. However, the linear temporal detection range for streak cameras operated in synchroscan mode is significantly less than the pulse repetition rate and, for most fluorophores of interest, the repetition rate of pulse trains from mode-locked lasers must therefore be reduced by means of a pulse-picker, further increasing the cost and complexity of such systems.

We report a novel TCSPC approach using a multi-element photomultiplier detector to record, in parallel, the fluorescence decay from each of 16 excitation beams in a multifocal multiphoton microscope. The repetition rate of the laser system used is 80 MHz and therefore each detector

channel has the potential to record photon events at up to ~3.2 MHz with a ~1% level of error in the measured lifetime [**32**]. Thus the maximum achievable photon detection rate for the whole system would exceed 50 MHz when using multiple electronic detection modules. Here we demonstrate this multibeam FLIM approach using a single TCSPC module that has a dead time of 125 ns. Therefore, at a count rate of 1 MHz, the efficiency with which photon events are recorded by the TCSPC electronics is ~88%. Higher count rates and higher photon detection efficiencies could be readily achieved through the use of multiple TCSPC detection modules for a bright sample.

2. Experimental setup

The microscope system used in this work consists of an electronically tunable Ti:Sapphire laser (Broadband MaiTai, Newport Spectra-Physics) coupled to a combined “prechirp” dispersion compensation, beam splitting and scanning unit (TriMScope, LaVision Biotec), see **Fig. 1**. The prechirp unit is configured to compensate for dispersion in the beam splitter and microscope optics. The beam splitting unit [**24**] was configured to produce 16 equally spaced beams that were coupled into an inverted microscope (IX71, Olympus) via a dichroic beamsplitter. The beam splitter also introduces a temporal delay between adjacent beams that is greater than the pulse duration; this ensures that there is no cross-talk between foci that could otherwise cause the axial resolution to be degraded [**38**].

For all of the results presented in this paper, a 63x oil immersion objective (HCX PL APO, Leica) was used that, together with the Olympus tube lens mounted in the IX71 microscope frame, resulted in a 56.7x magnification. The resulting fluorescence was then imaged via relay optics onto a 16 element stripe photomultiplier array (PML16, Becker & Hickl GmbH) connected through routing electronics to a TCSPC electronics module (SPC-830, Becker & Hickl GmbH). The active area of the PML16 consists of an array of 16 channels, each with dimensions 0.8×16 mm. The centre to centre spacing of the detector elements is 1 mm giving a total detector size of 16×16 mm.

The 16 foci were adjusted such that the inter-beam separation was 2.5 µm at the sample and such that the position of the fluorescence generated by each beam was imaged (with a 1 mm spacing between adjacent foci) to the centre of each stripe of the 16 channel detector. The foci were scanned in the direction perpendicular to the line of foci such that the generated fluorescence spots were scanned along the centre of each rectangular detector element. To acquire a complete image, the sample was then stepped in the direction parallel to the line of foci using a motorized microscope stage (ScanIM, Märzhäuser Wetzlar GmbH & Co. KG). This arrangement avoids the need to descan the fluorescence and therefore reduces the number of optical elements required in the emission beam path. In particular, this arrangement removes the requirement for optics that are highly reflective (or antireflection coated) at both the excitation and emission wavelengths and therefore

allows efficient collection of the fluorescence. One disadvantage of this configuration is that any non-uniformity in the sensitivity across any one detector element would be manifest in the final image. In practice, however, we did not find this effect to be a problem. If necessary, this effect could be corrected through calibration and the use of appropriate software. Alternatively, it is possible to avoid this effect by modifying the system to include cylindrical optics to produce an image of the sample in the direction parallel to the line of foci and to produce a stationary image of the back focal plane of the microscope objective (Fourier plane of the sample) in the direction orthogonal to the line of foci.

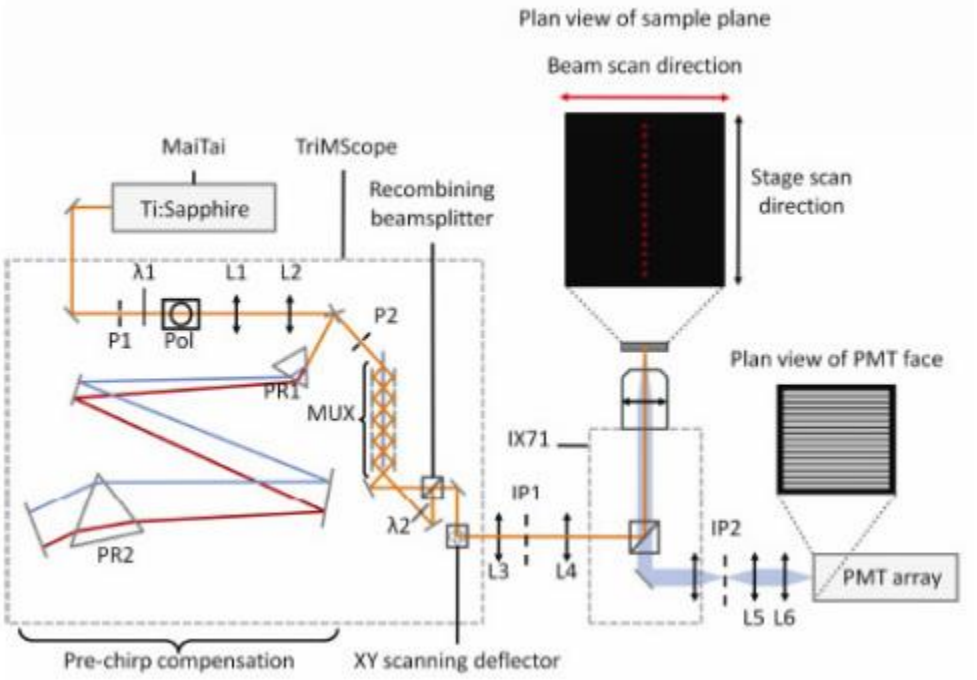

Fig. 1. Experimental setup: P1, P2 are pinholes, λ1,λ2 are half wave plates, L1-L6 are lenses, PR1, PR2 are prisms, MUX is the beam multiplexer, Pol is a rotatable polarizing beamsplitter cube and IP1, IP2 are image planes.

As the foci were scanned in the direction perpendicular to the line of foci, the fluorescence signal excited at each focus was imaged onto a corresponding element of the PMT array and was recorded as a function of time. If the excitation foci were scanned over *x* pixels, then a 16×*x* pixel TCSPC FLIM image would be recorded. This process was repeated as the sample was stepped by a fraction of the inter-focal distance in the direction parallel to the line of foci until sufficient (*y*) stage steps had been taken to build up a complete image of the sample. The resulting *y* TCSPC datasets were then interleaved in software to create a 16*y*×*x* pixel TCSPC image. We note that, since the spacing of the foci changes with the magnification, the microscope objective and field of view can be varied without needing to change the relay optics in front of the multi-anode PMT.

Figure 2 shows images acquired of fluorescently labelled pollen grains. The line of 16 foci was continuously scanned across the sample over 11.5 ms in the forward (acquisition) direction, and over 2.3 ms in the return (fly-back) direction, with the number of pixels being set to 256 in software, resulting in an effective pixel dwell time of 40 µs per pass for each beam. The fluorescence signal was integrated for 0.5 s at each position of the microscope stage. Detected photon events were routed to the correct bin in the histogram memory using electronic frame, line and PMT channel synchronization and routing signals. The stage was stepped 25 times in 100 nm steps in order to create a 400×256 image with a time resolution of 6 bits (64 time bins) in a total frame acquisition time of approximately 20 s; the discrepancy between the total acquisition time of 20 s and the actual data integration time of 12.5 s is due to the starting, stopping and reading out of the TCSPC card and movement of the microscope stage between each step. An image stack of 150 optically sectioned images was acquired in approximately 50 minutes and was used to produce the 3-D FLIM rendering shown in **Fig. 2(c)**. The excitation intensity was adjusted to give a count rate of 2.4 MHz which, given the dead time of the electronics following detection of a photon event of 125 ns, allows 70% of photon events to be detected.

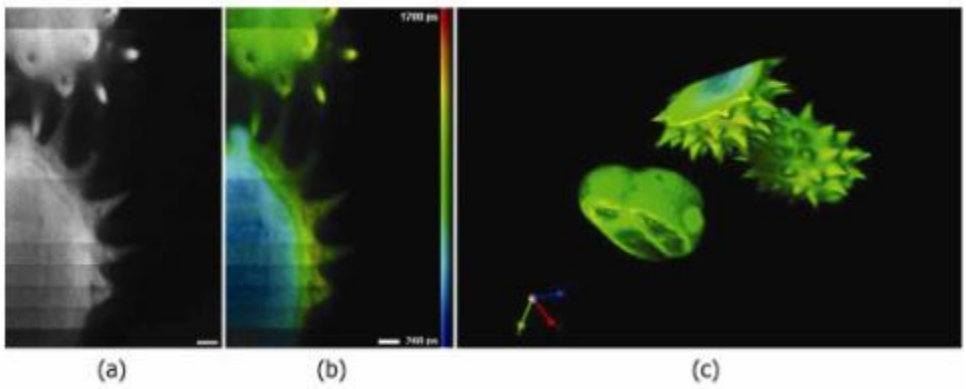

Fig. 2. 3-D FLIM image of fluorescently labelled pollen grains. (a) fluorescence intensity and (b) intensity-merged false-colour FLIM map for one slice in the image stack. (c) shows a single movie frame of a 3-D rendering [1561 KB] of the whole FLIM image stack using the same false colour scale as used for (b). λ_{ex} = 800 nm and the excitation power was set to P_{ex} = 1 mW per beam, which corresponded to a count rate of ~2.4 MHz. Scale bars in (a) and (b) are 2.5 µm and the data volume rendered in (c) is 25.6×40×75 μm^3. [**Media 1**]

The performance of this multifocal multiphoton FLIM microscope was to some extent impacted by the non-ideal properties of the photomultiplier array. For example, there was a small variation in sensitivity between anodes, which, together with a small variation in intensity between excitation foci, produced the weak horizontal striping effect of the images shown in **Fig. 2**. If necessary, this variation could be calibrated and the striping effect removed during data processing. Another potential issue is cross-talk between adjacent detector elements, which is indicated by the

manufacturer to be ~3%. We measured the cross-talk by imaging of a thin fluorescent film of rhodamine dye solution dried onto a microscope coverslip and found it to be 4% for our system. In principle, the effects of cross-talk could be removed using appropriate data processing but we did not consider this necessary for the results presented here. A further issue is the temporal instrument response function (IRF) of each anode. This was measured by recording the signal from femtosecond pulses that were frequency doubled in a beta barium borate (BBO) second harmonic generation (SHG) crystal placed at the focus of the microscope objective. Each of the detector elements has a similar temporal IRF profile but they exhibit slightly different temporal offsets. This temporal IRF data was used during data processing to correct data from individual detector channels by shifting the decays by an appropriate number of time-bins such that the temporal response was uniform across the entire image.

3. Multifocal multiphoton 3-D FLIM of GFP labelled NK cells

To demonstrate the multifocal TCSPC system applied to biological samples, we acquired image stacks of cells from a Natural Killer cell line, YTS, that have been transfected to express KIR2DL1-GFP. This biological system has been used previously for 3-D FLIM-FRET experiments [**9**, **39**]. Cells were sandwiched between a microscope slide and coverslip and imaged at room temperature. Each optically sectioned image was acquired in 60 s and an image stack consisting of 25 slices was acquired, see **Fig. 3**. The extent of photobleaching was observed to be ~18% between successive acquisitions of 3-D image stacks of the same cell.

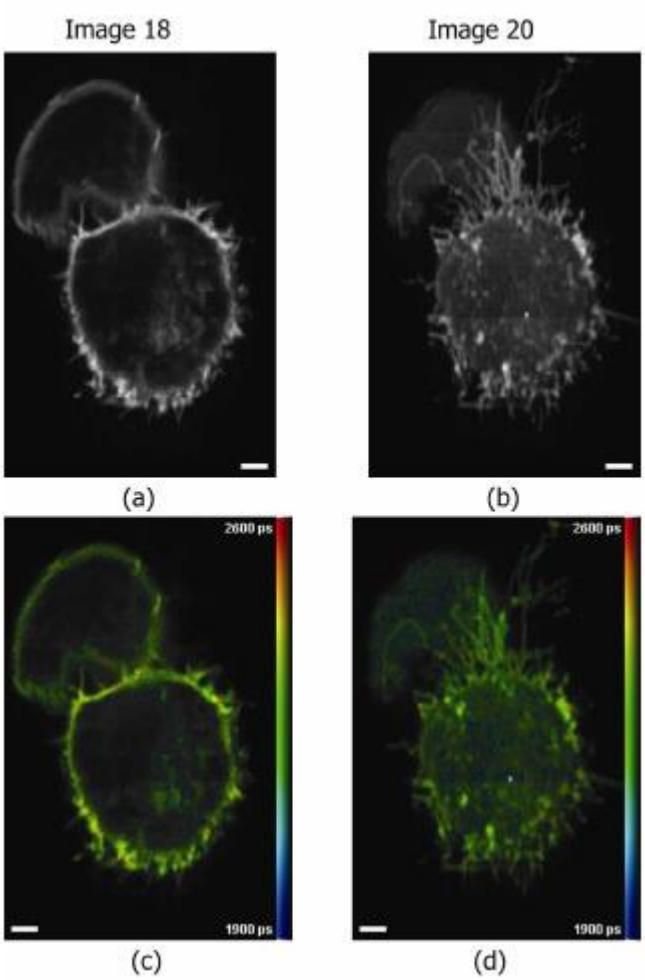

Fig. 3. (a-b) fluorescence intensity and (c-d) corresponding intensity-merged false-colour FLIM image of KIR2DL1-GFP expressing YTS cells. A total of 25 optically sectioned images were recorded using an acquisition time of 60 s per slice with λ_{ex} = 880 nm and an excitation power of 3.8 mW per foci. The field of view for this image was 25.6×40 μm with a z-step of 0.5 μm between consecutively numbered images. Scale bars are 2.5 μm.

This system provides a 16-fold increase in signal compared to using only a single beam on the same system when the power per focus is kept constant. In the case of the relatively weak fluorescence from these GFP-expressing cells, the photon detection rate is limited by the brightness of the sample, rather than the TCSPC electronics. For the measurements shown in **Fig. 3**, we employed an excitation power of 3.8 mW per beam, which is comparable to power levels commonly used for single beam multiphoton microscopy.

4. Multifocal multiphoton time-lapse lifetime imaging of cellular NAD(P)H autofluorescence

Cellular autofluorescence originating from reduced nicotinamide adenine dinucleotide (NADH) has been studied using multiphoton microscopy in the 720–760 nm range by a number of authors, e.g. [**3**, **40–42**]. Typically, the imaging rate is limited by non-linear photobleaching effects [**10**, **12**] and, in the case of live cell imaging, by the desire to minimize photodamage and phototoxicity [**18**, **43**]. Recently there has been interest in fluorescence lifetime measurements of cellular NADH autofluorescence, for detecting changes in cellular metabolism [**44–47**], and particularly those caused by cancer [**48**, **49**]. Here we demonstrate time-lapse multifocal multiphoton TCSPC FLIM applied to studying autofluorescence of NADH in single live cells.

NADH has a single-photon excitation peak at 340 nm, emitting blue fluorescence centred at 460 nm, and is the principal electron donor within the cell for both oxidative phosphorylation (aerobic respiration) and glycolysis (anaerobic respiration). NADPH (a molecule differing from NADH by the addition of a phosphate group) has identical excitation and emission spectra to NADH but is instead involved with transporting energy for anabolism (biosynthesis) within the cell. Previous work has shown that cellular NADPH fluorescence is weaker than that of NADH and can be normally assumed to be constant with respect to metabolic perturbations (see [**45**] and references therein). Cellular autofluorescence excited in the region of 340 nm is often termed NAD(P)H fluorescence, as the two species cannot be distinguished via their fluorescence excitation and emission spectra. Energy carried by reduced NADH is released through oxidation to NAD^+, which exhibits a very low fluorescence quantum yield at 340 nm compared to NADH [**50**]. Changes in the ratio of [NADH] to [NAD^+] can therefore be observed through changes in the fluorescence intensity of NAD(P)H [**51**].

The fluorescence lifetime of protein bound NADH is longer than that of free NADH and lifetime measurements have therefore been proposed as a method of monitoring the ratio of free to protein bound NADH. However, it is important to note that the analysis of the fluorescence decay of cellular NADH is not straightforward. Free NADH in aqueous solution at room temperature exhibits a bi-exponential fluorescence decay with fluorescence lifetime components of ~0.3 and ~0.7 ns [**45**, **52–54**] and a mean fluorescence lifetime of ~0.4 ns. Protein bound NADH also exhibits a bi-exponential fluorescence decay [**52**, **55**] and the shorter lifetime component can be comparable to that of the long lifetime component of free NADH. Therefore, the common practice of fitting a bi-exponential decay profile to a mixture of free and protein bound NADH exhibiting 4 decay components (or more, with multiple bound proteins) is a considerable simplification of the underlying dynamics. The change in the distribution of proteins bound to NADH during hypoxia has been attributed to the binding of NADH to proteins required for glycolysis, as opposed to oxidative phosphorylation [**45**] and this results in a shift in mean lifetime.

4.1 Experimental method

For autofluorescence imaging, HEK293a cells were plated onto glass-bottomed tissue culture dishes (Wilco) and cultured in Dulbecco's Modified Eagle's Medium supplemented with 10% Foetal Calf Serum, 4500 mg.ml^{-1}glucose and sodium pyruvate and 100 µg.ml^{-1} penicillin and streptomycin under 5% CO_2 at 37°C. Prior to imaging, the growth medium was replaced with 2 ml of Hanks Balanced Salt Solution (HBSS) and the cells were allowed to thermally equilibrate on the microscope stage for 10 minutes. Both the microscope stage and the microscope objective were maintained at 37°C throughout all experiments. Transmitted light images were used to locate individual cells and were acquired before and after multiphoton imaging. Multifocal multiphoton TCSPC imaging was performed with an excitation wavelength of 740 nm. The average excitation power was set to be 17.3 mW at the back aperture of the microscope objective, corresponding to 1.1 mW per focus and imaging was carried out with 1 s of integration per stage-step and 5 stage-steps of 500 nm per frame, giving a frame time of 7.7 s. This power level was determined to be suitable for long term multiphoton imaging by monitoring HEK293 cell morphology during illumination by the excitation laser at various power levels. Imaging at this excitation power level caused no significant photobleaching for continuous imaging for over 9 minutes and no significant morphological changes were observed. The relative fluorescence signal was found to be 0.97±0.04 (n=6) of the initial signal after 540 s of continuous acquisition at an average count rate of 3400 photons.s^{-1} per cell. **Figure 4** shows a typical transmitted light image of a HEK293 cell and the corresponding autofluorescence intensity image.

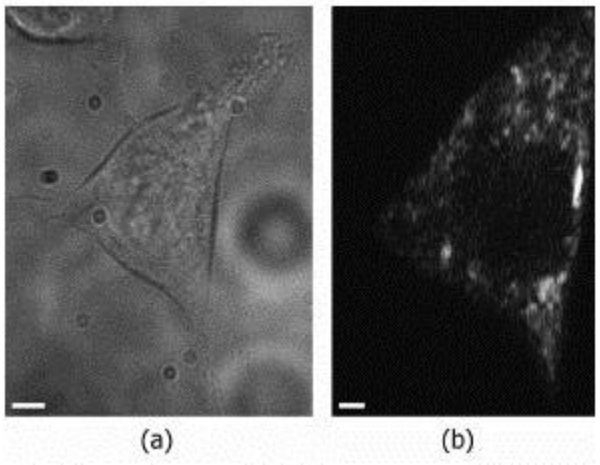

Fig. 4. (a). transmitted light image and (b) corresponding autofluorescence intensity image (averaged over 3 frames) of a HEK293 cell; image size is 80x256 pixels and the field of view is 40×25.6 µm Scale bars in both images are 2.5 µm.

For each time-lapse experiment, an initial 40 frames were acquired to allow the baseline fluorescence to be recorded. At frame 40, a control injection of 40 µl of HBSS was added to the

culture dish to verify that the injection of fluid did not cause any movement of the cell or change in fluorescence signal. Injection of a ‘stimulant’ was performed at frame 60 and the autofluorescence signal was then monitored for a further 20–50 frames. The ‘stimulant’ injection consisted of either a second injection of 40 µl HBSS or addition of 5 mM NaCN (stated concentration is the final concentration in the tissue culture dish). NaCN is a known metabolic inhibitor and evokes a response equivalent to hypoxia, thus minimizing the rate of oxidative phosphorylation, maximizing the concentration of NADH and therefore causing an increase in the NADH fluorescence intensity. As a control we also substituted the second injection by a 1 µm change in focal position of the sample to validate the experimental procedure. The change in focus causes a random step change in fluorescence intensity, as a different region of the cell is then imaged. This control verifies that there is no change in the measured fluorescence lifetime when there is a change in fluorescence intensity, as is confirmed in **table 1**.

It was not possible to calculate the fluorescence lifetime for each pixel of an image due to the low fluorescence signal. Therefore, a region of interest (ROI) was defined around each individual cell and the average fluorescence decay profile was extracted over the ROI for each frame of the time-lapse acquisition. The resulting fluorescence decay series was then fitted using SPCImage fitting software (Becker & Hickl GmbH). Due to a relatively high background count rate from the multichannel PMT (~600 counts.element$_{-1}$.s^{-1}) it was necessary to include a fixed offset in the fitting model. This offset was calculated from a ROI of a dark part of the image. A double exponential decay with this fixed offset was then fitted to the fluorescence data within the bounds shown in **Fig. 5**, to provide a measurement of the mean fluorescence lifetime. **Figure 5** shows an example of a fluorescence decay and the corresponding fit to the data. For the time lapse experiments, the fitted decay parameters were then plotted as a function of frame number, as shown in **Fig. 6**.

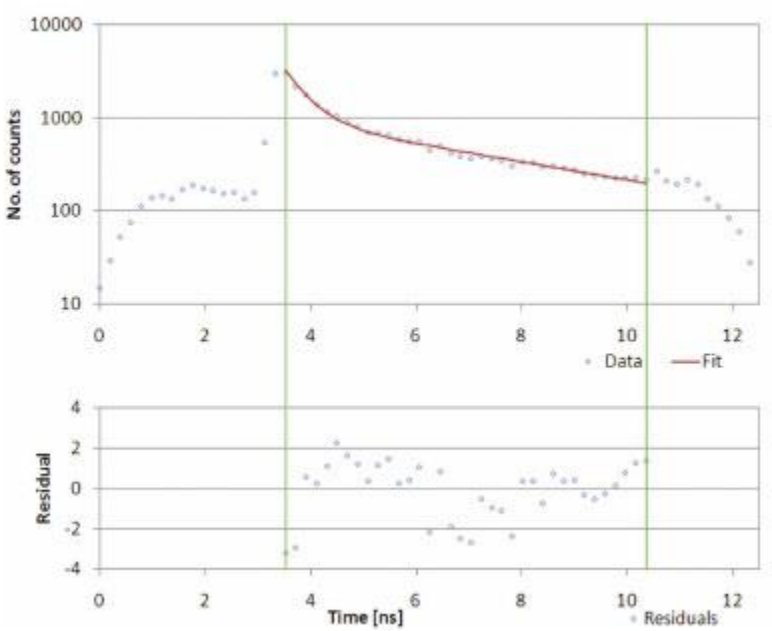

Fig. 5. Fluorescence decay profile averaged over an individual HEK293 cell from a single (7.7 s) acquisition frame and fit using a double exponential decay model. The bottom part of the figure shows the residuals of the fit.

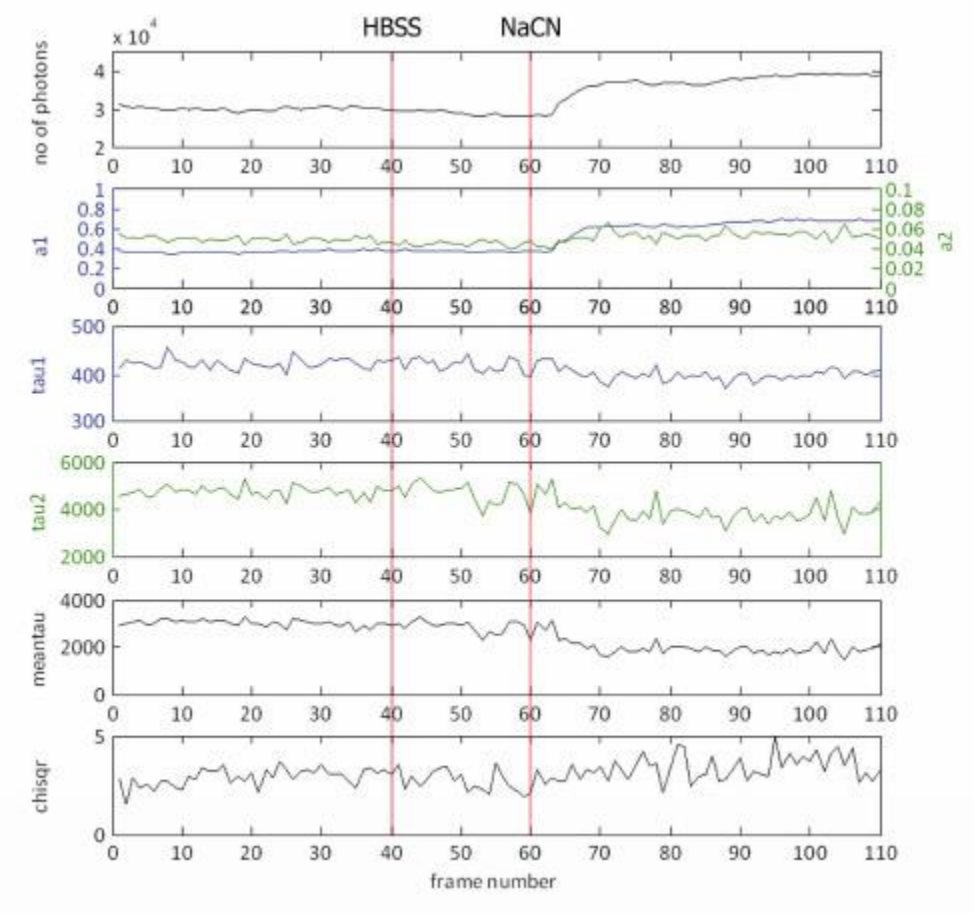

Fig. 6. Fitted time-lapse decay parameters for a HEK293a cell stimulated by 5 mM NaCN at frame 60. Each frame corresponds to 7.7 s. The graphs show (from top to bottom) total number of counts over the ROI, the pre-exponential factors (a1 and a2), the fluorescence decay lifetimes (tau1 and tau2), the calculated mean fluorescence lifetime (meantau) and the goodness of fit parameter χ^2 (chisqr). The vertical red lines indicate the time points at which HBSS and NaCN were added.

We note that this double exponential decay approximation was not entirely satisfactory. The measured background level did not provide the minimum value of χ^2 when fitting a double exponential decay model and, by binning together data from multiple image frames, it was apparent that the decay was not a true bi-exponential. We also investigated a triple exponential fit to the NAD(P)H decay, which yielded the same overall trends in mean fluorescence lifetime as the double exponential fit, but with a larger variation in the resulting mean lifetime (results not shown). For this demonstration experiment and within the limits of our data, we judged the mean lifetime from the double exponential decay fit to provide the most useful indication of changes in metabolic activity.

In order to quantify the changes in the fluorescence decay profile, the fitted fluorescence decay parameters were averaged before (frames 45–55) and after (frames 70–80) stimulation and the results are summarized in **table 1**.

Stimulant	Number of cells	Relative change in fluorescence intensity; I_{after}/I_{before} (±σ)	Relative change in τ_{mean}, $\tau_{after}/\tau_{before}$ (±σ)
Control	6	0.99 (0.04)	1.00 (0.04)
Focal shift	4	1.01* (0.03)	0.99 (0.03)
5 mM NaCN	5	1.16 (0.11)	0.80 (0.10)

Table 1. Summary of changes in autofluorescence signal observed before and after stimulation

Stimulation with 5 mM NaCN evokes the expected increase in fluorescence intensity and also produces a decrease in the mean fluorescence lifetime, which is in agreement with other results [**45**, **47**, **49**]. We note that the small number of cells (n=5) used in this study is not sufficient to draw conclusions on this data alone.

5. Discussion and Conclusion

We present the first multifocal multiphoton FLIM microscope using TCSPC, where the fluorescence decay profiles from each of the excitation foci are recorded individually in a light-efficient non-descanned detection scheme. This approach is particularly suited to acquiring high resolution 3-D FLIM datasets, benefiting from 1) low out-of-focus photobleaching via multiphoton excitation, 2) increased rate of fluorescence signal acquisition through the use of multiple excitation beams and 3) photon efficient and robust time-resolved detection of the fluorescence signal using TCSPC electronics. With bright fluorescent samples, the use of up to 16 TCSPC electronics modules to provide count rates up to ~ 50 MHz could provide significantly faster imaging than is possible with a single beam microscope without increasing fluorophore photobleaching or saturation. With weakly fluorescent samples, the multiple foci provide an enhanced fluorescence signal and only a single TCSPC module is required.

Although this first implementation of our multifocal multiphoton TSCPC FLIM microscope works well, there is scope for improvement. The speed of image acquisition could be improved by eliminating the need for stage scanning. This could be achieved by translating both the line of excitation foci, using the scanning mirrors, and simultaneously translating either the detector or the path of the detected signal using an additional scanning mirror. Alternatively, the need for sample stage scanning could be removed by realising true multifocal descanned detection [**56**, **57**], although this

would require the scanning mirrors and lenses, which are currently optimized for IR, to be replaced in our system in order to achieve a useful fluorescence detection efficiency. For the non-descanned geometry, we note that it would also be possible to place a narrow slit aperture in front of each element of the photomultiplier array in order to reduce optical cross-talk when imaging through scattering samples. For quantitative imaging, it may be desirable to calibrate and compensate in data processing for electrical cross-talk between photomultiplier elements and for variations in sensitivity along the stripe detectors and between the different elements. If the sensitivity and noise properties of the photomultiplier array detector could be improved, this would directly benefit the performance and imaging rate of this microscope system. Finally, the functionality of this system could be extended to image time-resolved fluorescence anisotropy decay profiles using either rapid switching of the polarization of the excitation beams or by polarisation-splitting the fluorescence signal onto two 16 channel photomultiplier array detectors.

In its current form, the system is capable of acquiring data up to 16 times faster than a single beam system on samples exhibiting relatively weak fluorescence or, more specifically, for samples where photodamage or photobleaching considerations limit single beam count rates to on the order of 10^5 counts per second. Low levels of fluorescence signal are not uncommon when imaging genetically expressed fluorophores, where one concern is to retain a physiological level of expression of the tagged protein(s). The conversion of the system to use multiple TCSPC detection modules would require modifications to the electronics hardware. The detector used in this work incorporates integrated routing electronics, which would need to be modified or removed if multiple detection modules were to be employed. While the cost of individual TCSPC detection modules is relatively high, the cost per module decreases when sets of multiple modules are purchased.

By way of demonstration of the system, we acquired 3-D image stacks of fluorescently labelled pollen grains, using the single TCSPC module available to us, and demonstrated 3-D FLIM. The frame data acquisition time with this sample could be further reduced to below one second using 16 TCSPC modules. To illustrate the potential for cell biology applications such as 3-D FLIM-FRET, we acquired FLIM image stacks of live YTS cells expressing KIR2DL1-GFP. We also applied this multifocal multiphoton FLIM microscope to endogenous NADH fluorescence in individual cells, for which photobleaching and phototoxicity considerations limit the maximum usable excitation power. Through continuous time-lapse acquisitions of NAD(P)H autofluorescence from HEK293 cells, we showed that it is possible to follow the autofluorescence decay profile dynamics of individual cells following stimulation with NaCN. This is relevant to detecting changes in cellular metabolism using endogenous fluorescence and our results agree with previous studies of the fluorescence lifetime of NAD(P)H. In particular, this result highlights the ability of the system to follow dynamic changes in fluorescence lifetime and simultaneously observe the spatial distribution of the fluorescence signal. In the future, this experiment could yield information on the rate at which cellular respiration shifts

from oxidative phosphorylation to glycolysis following stimulation and provide this information for multiple cells in the field of view simultaneously. In general, monitoring changes in fluorescence lifetime has the potential to provide additional and more quantitative information on the state of cellular metabolism compared to monitoring only the fluorescence intensity. We note that, while the parallel multifocal excitation provides a greater autofluorescence signal for a given level of photobleaching compared with a single beam excitation, a more detailed investigation is required to compare the relative phototoxicity of multiple excitation beams over long time-lapse acquisitions with respect to single beam excitation.

REFERENCES

[1] Kumar, S., 2015, "Fundamental limits to Morre's law", arXiv:1511.05956, http://arxiv.org/abs/1511.05956

[2] D. V. O'Connor and D. Phillips, *Time-correlated single-photon counting* (Academic press, London, 1984).

[3] H. C. Gerritsen, M. A. H. Asselbergs, A. V. Agronskaia, and W. Van Sark, "Fluorescence lifetime imaging in scanning microscopes: acquisition speed, photon economy and lifetime resolution," J. Microsc. **206**, 218–224 (2002).

[4] W. Becker, A. Bergmann, M. A. Hink, K. Konig, K. Benndorf, and C. Biskup, "Fluorescence lifetime imaging by time-correlated single-photon counting," Microsc. Res. Tech. **63**, 58–66 (2004).

[5] R. V. Krishnan, H. Saitoh, H. Terada, V. E. Centonze, and B. Herman, "Development of a multiphoton fluorescence lifetime imaging microscopy system using a streak camera," Rev. Sci. Instrum. **74**, 2714–2721 (2003).

[6] J. L. Qu, L. X. Liu, D. N. Chen, Z. Y. Lin, G. X. Xu, B. P. Guo, and H. B. Niu, "Temporally and spectrally resolved sampling imaging with a specially designed streak camera," Opt. Lett. **31**, 368–370 (2006).

[7] Suhas, K, Sripadaraja, K, "Mechanical modeling issues in optimization of dynamic behavior of RF MEMS switches," 2008, Int. J. Comp. Inform. Syst. Sci. Eng., 221-225.

[8] Suhas, K., "Modelling Studies and Fabrication Feasibility with LTCC for Non-Conventional RF MEMS Switches," 2007, IISC.

[9] D. S. Elson, I. Munro, J. Requejo-Isidro, J. McGinty, C. Dunsby, N. Galletly, G. W. Stamp, M. A. A. Neil, M. J. Lever, P. A. Kellett, A. Dymoke-Bradshaw, J. Hares, and P. M. W. French, "Real-time time-domain fluorescence lifetime imaging including single-shot acquisition with a segmented optical image intensifier," New J. Phys. **6**, 13 (2004).

[10] Kumar, S., Esfandyarpour, R., Davis, R., Nishi, Y., "Charge sensing by altering the phase transition in VO2," APS March Meeting Abstracts 2014, 1, 1135.

[11] Kumar, S., Esfandyarpour, R., Davis, R., Nishi, Y., "Surface charge sensing by altering the phase transition in VO2," Journal of Applied Physics 2014, 116, 074511.

[12] W. Becker, *Advanced Time-Correlated Single Photon Counting Techniques* (Springer, Berlin, 2005).

[13] C. J. de Grauw and H. C. Gerritsen, "Multiple time-gate module for fluorescence lifetime imaging," Appl. Spectrosc. **55**, 670–678 (2001).

[14] M. Straub and S. W. Hell, "Fluorescence lifetime three-dimensional microscopy with picosecond precision using a multifocal multiphoton microscope," Appl. Phys. Lett. **73**, 1769–1771 (1998).

[15] S. Leveque-Fort, M. P. Fontaine-Aupart, G. Roger, and P. Georges, "Fluorescence-lifetime imaging with a multifocal two-photon microscope," Opt. Lett. **29**, 2884–2886 (2004).

[16] Kumar, S., "Fundamental limits to Moore's law," 2012, Stanford University

[17] A. K. Mondal, S. Kumar, C. Blawert, N. B Dahotre, *Effect of laser surface treatment on corrosion and wear resistance of ACM720 Mg alloy*, Surface and Coatings Technology, 2008, 202, 3187

[18] Aslani, M., Garner, C. M., Kumar, S., Nordlund, D., Pianetta, P., Nishi, Y., "Characterization of electronic structure of periodically strained graphene," Appl. Phys. Lett., 2015, 107 (18), 183507.

[19] Gerke, A, Kumar S., Provine, J., Saraswat K., "Characterization of metal-nitride films deposited by the Savannah ALD system," Stanford University.

[20] R. K. P. Benninger, O. Hofmann, J. McGinty, J. Requejo-Isidro, I. Munro, M. A. A. Neil, A. J. deMello, and P. M. W. French, "Time-resolved fluorescence imaging of solvent interactions in microfluidic devices," Opt. Express **13**, 6275–6285 (2005).

[21] Suhas, K, "Materials and processes in 3D structuration of low temperature cofired ceramics for meso-scale devices," Industrial Ceramics, 2010, 30(1).

[22] L. Liu, J. Qu, Z. Lin, L. Wang, Z. Fu, B. Guo, and H. Niu, "Simultaneous time- and spectrum-resolved multifocal multiphoton microscopy," Appl. Phys. B-Lasers and Optics **84**, 379–383 (2006).

[23] A. Egner and S. W. Hell, "Time multiplexing and parallelization in multifocal multiphoton microscopy," J. Opt. Soc. Am. A-Opt. Image Sci. Vis. **17**, 1192–1201 (2000).
[24] Kumar, S., "Atomic Batteries: Energy from radioactivity," 2015, arXiv:1511.07427, http://arxiv.org/abs/1511.07427
[25] Kumar, S., "Energy from radioactivity," 2011, Stanford University
[26] P. D. Borszcz, M. Peterson, L. Standeven, S. Kirwan, M. Sandusky, A. Shaw, E. O. Long, and D. N. Burshtyn, "KIR enrichment at the effector-target cell interface is more sensitive than signaling to the strength of ligand binding," Eur. J. Immunol. **33**, 1084–1093 (2003).
[27] Kumar, S, "Learning from Solar Cells - Improving Nuclear Batteries,", 2012, Stanford University,
[28] B. R. Masters, P. T. C. So, and E. Gratton, "Multiphoton excitation fluorescence microscopy and spectroscopy of in vivo human skin," Biophys. J. **72**, 2405–2412 (1997).
[29] Kumar, S., "Superconductors for electrical power," 2011, Stanford University
[30] G. H. Patterson, S. M. Knobel, P. Arkhammar, O. Thastrup, and D. W. Piston, "Separation of the glucose-stimulated cytoplasmic mitochondrial NAD(P)H responses in pancreatic islet beta cells," Proc. Natl. Acad. Sci. U. S. A. **97**, 5203–5207 (2000).
[31] Kumar, S., "On the Thermoelectrically Pumped LED," 2012, Stanford University
[32] S. H. Huang, A. A. Heikal, and W. W. Webb, "Two-photon fluorescence spectroscopy and microscopy of NAD(P)H and flavoprotein," Biophys. J. **82**, 2811–2825 (2002).
[33] M. G. Nichols, E. E. Barth, and J. A. Nichols, "Reduction in DNA synthesis during two-photon microscopy of intrinsic reduced nicotinamide adenine dinucleotide fluorescence," Photochem. Photobiol. **81**, 259–269 (2005).
[34] Kumar, S, "Mechanisms of resistance switching in various transition metal oxides," Thesis, Stanford University (2014)
[35] Jayamurugan, G, Vasu, K. S., Rajesh, Y. B. R. D., Kumar, S., Vasumathi, V., Maiti, P. K., Sood, A. K., Jayaraman, N., "Interaction of single-walled carbon nanotubes with poly (propyl ether imine) dendrimers,", J. Chem. Phys. 2011, 134, 104507.
[36] M. Hazara, A. K. Mondal, S. Kumar, C. Blawert, N. B Dahotre, *Laser surface cladding of MRI 153M magnesium alloy with (Al+ Al 2 O 3)*, Surface and Coatings Technology, 2009, 203, 2292
[37] H. Schneckenburger and K. Konig, "Fluorescence Decay Kinetics and Imaging of Nad(P)H and Flavins as Metabolic Indicators," Opt. Eng. **31**, 1447–1451 (1992).
[38] H. D. Vishwasrao, A. A. Heikal, K. A. Kasischke, and W. W. Webb, "Conformational dependence of intracellular NADH on metabolic state revealed by associated fluorescence anisotropy," J. Biol. Chem. **280**, 25119–25126 (2005).
[39] D. K. Bird, L. Yan, K. M. Vrotsos, K. W. Eliceiri, E. M. Vaughan, P. J. Keely, J. G. White, and N. Ramanujam, "Metabolic mapping of MCF10A human breast cells via multiphoton fluorescence lifetime imaging of the coenzyme NADH," Cancer Res. **65**, 8766–8773 (2005).
[40] Y. C. Wu, W. Zheng, and J. N. Y. Qu, "Sensing cell metabolism by time-resolved autofluorescence," Opt. Lett. **31**, 3122–3124 (2006).
[41] Kumar, S, et. al., "Sequential electronic and structural transitions in VO2 observed using x-ray absorption spectromicroscopy," 2014, Advanced Materials, 26, 7505.
[42] A. Pradhan, P. Pal, G. Durocher, L. Villeneuve, A. Balassy, F. Babai, L. Gaboury, and L. Blanchard, "Steady state and time-resolved fluorescence properties of metastatic and non-metastatic malignant cells from different species," J. Photochem. Photobiol. B-Biol. **31**, 101–112 (1995).
[43] Kumar, S., "Types of atomic/nuclear batteries," 2012, Stanford University
[44] M. C. Skala, K. M. Riching, D. K. Bird, A. Gendron-Fitzpatrick, J. Eickhoff, K. W. Eliceiri, P. J. Keely, and N. Ramanujam, "In vivo multiphoton fluorescence lifetime imaging of protein-bound and free nicotinamide adenine dinucleotide in normal and precancerous epithelia," J. Biomed. Opt. **12**, 024014-024011-024010 (2007).
[45] A. Mayevsky and G. G. Rogatsky, "Mitochondrial function in vivo evaluated by NADH fluorescence: from animal models to human studies," Am. J. Physiol.-Cell Physiol. **292**, 5–C640 (2007).
[46] B. Chance, P. Cohen, F. Jobsis, and B. Schoener, "Intracellular Oxidation-Reduction States in Vivo," Science **137**, 499–508 (1962).
[47] Kumar, S, et. al., "Smart packaging of electronics and integrated MEMS devices using LTCC," 2016, arXiv:1605.01789
[48] A. Gafni and L. Brand, "Fluorescence Decay Studies of Reduced Nicotinamide Adenine Dinucleotide in Solution and Bound to Liver Alcohol Dehydrogenase," Biochemistry **15**, 3165–3171 (1976).
[49] A. J. W. G. Visser and A. van Hoek, "The fluorescence decay of reduced nicotinamides in aqueous solution after exciation with a UV-mode locked Ar Ion Laser," Photochem. Photobiol. **33**, 35–40 (1981).
[50] M. Wakita, G. Nishimura, and M. Tamura, "Some Characteristics of the Fluorescence Lifetime of Reduced Pyridine-Nucleotides in Isolated-Mitochondria, Isolated Hepatocytes, and Perfused-Rat-Liver in-Situ," J. Biochem.(Tokyo) **118**, 1151–1160 (1995).
[51] Kumar, S, et. al., "The phase transition in VO2 probed using x-ray, visible and infrared radiations," Applied Physics Letters, 2016, 108, 073102
[52] Kumar, S, et. al., 2013, "Local temperature redistribution and structural transition during Joule-heating-driven conductance switching in VO2," Advanced Materials, 2012,25, 6128.
[53] J. C. Brochon, P. Wahl, M. O. Monneuse-Doublet, and A. Olomucki, "Pulse Fluorimetry Study of Octopine Dehydrogenase-Reduced Nicotinamide Adenine Dinucleotide Complexes," Biochemistry **16**, 4594–4599 (1977).

[54] J. Martini, V. Andresen, and D. Anselmetti, "Scattering suppression and confocal detection in multifocal multiphoton microscopy," J. Biomed. Opt. **12**, 034010–034016 (2007).
[55] T. Ragan, J. D. Sylvan, K. H. Kim, H. Huang, K. Bahlmann, R. T. Lee, and P. T. C. So, "High-resolution whole organ imaging using two-photon tissue cytometry," J. Biomed. Opt. **12**, 9 (2007).